Electric Power Systems Research 221 (2023) 109460

Contents lists available at ScienceDirect

Electric Power Systems Research

journal homepage: www.elsevier.com/locate/epsr

Enabling resiliency using microgrids with dynamic boundaries

Illia M. Diahovchenko [a,b,*], Gowtham Kandaperumal [c], Anurag K. Srivastava [d]

[a] Department of Electrical Power Engineering, Sumy State University, Sumy, 40007, Ukraine
[b] Institute for Research in Technology, ICAI, Comillas Pontifical University, Madrid, 28045, Spain
[c] Senior Engineer, Commonwealth Edison, Chicago, IL, 60605, United States of America
[d] Lane Department of Computer Science and Electrical Engineering, West Virginia University, Morgantown, WV, 26506, United States of America

ARTICLE INFO

Keywords:
Power system resiliency
Analytic hierarchy process
Automated switches
Distributed energy resources
Graph theory
Microgrid with dynamic boundaries

ABSTRACT

With the increased frequency of adverse weather and manmade events in recent years, the issue of the power distribution system (PDS) resiliency has become drastically important. Microgrids with various types of distributed energy resources (DERs) have capabilities to enhance the PDS's resiliency against high impact low probability (HILP) events. Resiliency is defined as the ability of the system to keep supplying critical loads even during and after extreme contingencies. This paper presents a systematic method to segmentize parts of a PDS into microgrids with flexible boundaries to enhance resiliency and mitigate negative impacts from anticipated threats. The method is aimed at anticipation and preparation to HILP events in advance: alternative flexible boundaries of the microgrids must be preplanned during normal operation and dynamically changed prior to or during disturbances. The Mixed-Integer Linear Programming (MILP) is formulated and applied to select switching actions to adjust microgrids' boundaries as well as to supply critical loads, while meeting system constraints. Networked microgrids are merged and reconfigured as necessary to maximize supply to critical loads, driven by a factor-based resiliency metric, which is obtained using the Analytical Hierarchy Process (AHP). The modified IEEE 123 bus system was utilized for validation of the proposed method. Compared with the traditional fixed-boundary microgrids, this approach determines the most resilient network configuration to supply high-priority critical loads. The developed method can be employed in power system planning, operation, and in decision-making to enhance operational resiliency and invest in system upgrades appropriately.

1. Introduction

Weather events and cyber-attacks account for many power supply interruptions, reliability and resiliency issues. In recent years, the world endured several severe weather events, which resulted in power outages, blackouts, and dozens of billion dollars losses for economies. In the USA the 2012 hurricane Sandy caused a total of $71 billion in damages, the 2017 hurricane Maria caused $90 billion losses, and the 2017 hurricane Harvey lead to a severe harm of $125 billion [1]. The October 2015 typhoon, which hit Zhanjiang, China, caused a loss of 4.24 million kWh of energy [2]. The December 2015 synchronized and coordinated cyber-attack compromised three Ukrainian regional electric power distribution companies, and the following outages affected nearly 225 thousand customers [3]. The 2019 Venezuela blackout, alleged to be a foreign cyber-attack, plunged into darkness about 30 million people [4]. The February 2021 Taxes outage showed how an extreme winter storm could shake an entire community to its core, resulting in $195 billion in property damage and more than 4.5 million homes left without electricity [5]. And in 2022 and 2023 the missile attacks on power plants and infrastructure committed by russia destroyed 40% of the Ukrainian energy system, resulting in blackouts in most of the country and leaving millions of people in the dark [6,7]. Given the increasing frequency and severity of disastrous events, the PDS resiliency is becoming an imperative concern. While nearly 90% of all hurricane-related outages occur in distribution grids [8], the low-voltage consumers also lose electricity supply after damage of transmission lines and upstream substations, which is often the case after natural disasters or terroristic missile attacks on energy infrastructure [6,7]. After such HILP events several isolated areas may become unpowered. Therefore, the traditional load restoration methods (e.g., [9–12]), which entirely rely on reconfiguration and imply the energization from the utility, may not ensure continuous energy supply after unfavorable events, and some customers may face extended outages [2,13]. One solution to save critical loads (CLs) is the microgrid (MG), which can be determined as a group of

* Corresponding author.
E-mail address: i.diahovchenko@etech.sumdu.edu.ua (I.M. Diahovchenko).

https://doi.org/10.1016/j.epsr.2023.109460
Received 14 November 2022; Received in revised form 21 April 2023; Accepted 3 May 2023
Available online 25 May 2023

interconnected loads and DERs with clearly defined electrical boundaries that acts as a single controllable entity with respect to the grid [and can] connect and disconnect from the grid, enabling operation in both grid-connected and islanded mode [14]. Based on this definition, a microgrid is characterized by the following features [15].

- It has distinct electrical boundaries.
- It can operate in grid-connected or island mode.
- It forms an independent controllable entity.
- It comprises distributed generator(-s) and loads.

DERs are increasingly integrated with the distribution network due to their ability to mitigate high marginal network losses, relieve network congestion or defer impending upgrades, enhance reliability, and improve resiliency [16–19]. The expediency of DERs intentional islanding was reflected in IEEE 1547.4 [20]. Therefore, DERs facilitate microgrids formation, which can operate in an islanded mode to support internal customers in case of an outage, improving the resiliency of the distribution grid as a whole.

The value of MGs for power network resiliency improvement has been recognized, and the academic community has conducted extensive studies and reported them in the scientific literature [21]. The article [2] presents a MG formation method for load restoration after natural disasters, where the master-slave technique is implemented for DGs coordination. In [22] applications of genetic algorithm and particle swarm optimization techniques for reconfiguration of a shipboard MG are demonstrated. A decision-making service restoration strategy that coordinates multiple sources to energize CLs after blackouts is defined in [23]. The authors of [24] developed a synthetic model for distribution power network restoration and crew dispatch, which considers routing sequence of two types of crew and load energization sequence. A strategy for sequential service restoration, considering uncertainties associated with load demand and renewable energy sources was proposed in [25]. The paper [26] introduces a black start restoration algorithm that energizes the remote MG based on priority of critical load clusters. In [27] the application of Monte Carlo simulation is demonstrated to assess the resiliency of multi-microgrid-based power systems against probable devastating natural events. The work [28] introduces a novel tool to assess the cyber-physical security of MGs and to assist the operator with remedial control actions to strengthen resiliency. To reinforce the network against severe faults, the study [29] aims to optimize the location and generation capacity of future MGs, using heuristic and MILP-based approaches. In [30] the authors attract the readers' attention to the concept of networked microgrids, which is referred as a cluster of physically interconnected and functionally interoperable MGs, and review the state-of-the-art methodologies for their operation and control. A strategy to improve resiliency of large-scale distribution systems with networked MGs, considering the tradeoffs between upgrade costs and resiliency performance, is elaborated in [31].

Impermanence, weather dependence and stochastic nature of renewable-based dispersed generation can sophisticate their integration with the mains [32,33], which makes a fixed-boundary concept inadequate for resilient and efficient microgrid formation. To get over these limitations and to achieve the goal of dividing distribution networks into adaptive self-adequate MGs, the contemporary paradigm of a dynamic microgrid with shifting boundary was presented in [34], which facilitates the transition from a centralized large-scale system to a smart grid. The authors described the dynamic microgrid as "a MG with flexible boundaries that expend or shrink to keep the balance between generation and load at all times". Basing on the assessment of self-adequacy of each operating scenario, the clusters of nodes are to be selected, and a control agent is to be assigned to each cluster [34].

Various methods for PDSs partitioning have been proposed in scientific literature. A survey on the strategies and applications of microgrids with flexible boundaries is provided in [35]. The article [36] presents an approach to determine the operating modes of synchronous-machine DGs and the on-off statuses of smart switches, so as to change the boundaries of MGs network, aimed at fault isolation and restoration of de-energized loads. Dynamic reconfiguration of a MG can be achieved by operating of smart switches or associated switchgear, which can serve as the point of common coupling for temporary created MGs [30]. A controller to enable real-time operation of the MG with dynamic frontiers is proposed in [37]. The work [38] proposes a controller to synchronize the dynamic boundaries of MGs, based on the operation behavior of the dispersed generation inside the MG. The article [39] presents a two-layer mechanism to enhance the resiliency of a PDS with microgrids formation using weighted average consensus. This mechanism [39] detects the nodes that have faulted and/or lost their communication data and dynamically forms some of the microgrids' boundaries. The authors of [40] proposed a method to augment the resiliency of networks with unbalanced dynamic MGs using control of DGs' inverters. And a model-predictive-control-aided strategy for formation of dynamic-boundary MGs during an outage in the feeder is presented in [41].

As it was concluded in the survey [35], MGs with flexible boundaries have a high potential, but more research is required in this area. The outputs of the papers [2,21-23,27-29,31] are primarily focused on the conventional fixed-boundary MGs with fixed frontiers, which cannot be adjusted depending on the operational conditions. The studies [23–26] are aimed at quick service restoration and sequential service restoration after an outage and do not consider planning strategies to prepare the PDS for possible HILP events. In [27,34] the Monte Carlo Method is used, which is computationally expensive, i.e., a large number of samples is needed to obtain accurate results. The methods from [36–38] are not supported by any measures to quantify the improvements in the network's resiliency. In [40] it is not demonstrated how the proposed method can be adopted for resiliency-focused partition of dynamic MGs. Additionally, none of the previous papers [34–41] considered the concept of MGs with flexible boundaries as an option for pre-event resiliency-focused planning. In particularly, in [34] the authors aimed for self-adequacy of the MGs with flexible boundaries; the works [36,39] focused on the load service restoration at the post-disturbance stage; the articles [37,38,40] dealt with control strategies for MGs' reconfiguration and paid few attention to resiliency assessment; while the objective of the approach in [41] was to retain continuity of power supply during the disturbance stage.

To overcome the limitations of the previous studies, this paper presents a method to determine the optimal microgrid boundaries in advance, taking into account resiliency performance of each possible configuration. In contrast to the restoration and reconfiguration approaches, which tackle the post-event operation, this study proposes to preplan the flexible boundaries of the MGs so that they can be changed during normal operation, in anticipation of expected disturbances (planning decision-making domain). For this purpose, all the feasible configurations of the multi-microgrid PDS will be assessed and scaled according to their resiliency performance, which can be assessed with a composite metric. If a HILF event hits unexpectedly, the flexible boundaries of the MGs can be changed after the disturbance, which shifts decision-making to the operational domain. The adjustment of the MGs' boundaries will be triggered by an imbalance between the available power generation and power demand, with regard to resiliency-based estimated performance. Having resiliency scores, a distribution system operator (DSO) or automatics can choose the most resilient topology of the MGs with flexible boundaries; and system planners can get insights on where infrastructure hardening and/or flexible resource deployment are needed. Consequently, the contributions of this work are summarized as follows.

- Developed a comprehensive method for preplanned segmentation of the PDS into MGs with flexible boundaries to enhance resiliency and avoid disruptions of power supply to critical loads.

- Proposed a three-stage algorithm to enable resiliency of the PDS subjected to HILP events and/or multiple faults, using MILP.
- Assessed the impact of the controllable MGs with flexible boundaries on power system resiliency performance with a composite metric, which has been developed using system characteristics-based factors and AHP.

The rest of the paper is organized as follows. Section 2 outlines the optimal microgrids formulation problem. Section 3 describes the mechanism to form microgrids with dynamic boundaries with respect to the objective, which is to save the maximum fraction of consumers, taking into account loads' priority. In Section 4 numerical results for normal operation and recommendations for high network resiliency satisfaction are provided, followed by the PDS testing under an emergency scenario. The conclusions are stated in Section 5.

2. Problem formulation

The PDS is treated as a graph $G(N, E)$ with N vertices and a set of edges E so, that $E := \{(i, j)\} \subseteq N \times N$. To achieve the objective of resilient MGs with dynamic boundaries formation and to assure CLs restoration in case of a fault (or multiple faults), the following assumptions are made.

1 At each node $i \in N$, which consumes active and reactive power, there is a load denoted by p_i and q_i, respectively. For a node without any load, p_i and q_i are equal to zero. The power demand in the network should be predetermined for each operation scenario, basing on historical data. Thus, the formation of MGs with dynamic boundaries is affordable through consideration of multiple operating scenarios.
2 The optimal location of distributed generators (DGs) in the power system is predefined. DGs can feed multiple loads by forming microgrids, the set of which is denoted by M. Under this assumption, each MG $m \in M$ consists of a set of nodes N_m satisfying $N_m \subset N$ and $N_{m1} \cap N_{m2} = \varnothing$, $\forall m_1, m_2 \in M$. In case of a contingency, power outputs of several DGs can be combined to satisfy the goal of uninterrupted supply of CLs. The rated output power of each DG is denoted by p_m^{DG} and q_m^{DG}, respectively.
3 For ultimate control and flexibility, remotely controlled automatic switches and control agents should be installed at each node and at each line. However, it complicates the PDS and is economically impracticable [34]. Instead, pre-allocated representative control agents are assigned to all possible self-adequate clusters of nodes. These agents coordinate the DERs and isolation switches of the clusters, exchange information with neighboring clusters and provide a two-way communication with the smart meters of the consumers within the cluster [34]. Local communication between neighboring switches can be achieved by exploitation of wireless technologies like Wi-Fi or ZigBee [13]. If any two or more MGs are merged, then only one agent represents the entire microgrid, while other agents just collect and exchange data about load demand and generation ratings in their control area. Let $\beta_{ij} \in \{0, 1\}$ denote the binary decision variables for the isolation switch at the boundary of the clusters (in the branch between the nodes i and j). If the branch switch is closed ($\beta_{ij} = 1$), and if it is opened ($\beta_{ij} = 0$).
4 Additionally, automated switches are installed at all load nodes so that any consumer can be curtailed in case of emergency and/or shortage of available generation. Let $l_i \in \{0, 1\}$ denote the binary decision variables for switches connecting the load and the node i. For the closed load switch ($l_i = 1$), and for the opened load switch ($l_i = 0$), respectively.

3. Formation of microgrids with dynamic boundaries

The formation procedure being introduced in this section can be divided into three stages. The first stage (Section 3.1 and Section 3.2) presents the optimization formulation for microgrids with dynamic boundaries. There are limited options based on pre-planned boundaries to meet protection and other logistic constraints. M microgrids are shaped by controlling the automated switches and DERs' outputs by solving the mixed-integer linear programming formulation. The second stage (Section 3.3) defines the power flow constraints, which must be obeyed for network feasibility. The third stage (Section 3.4) introduces the resiliency-driven decision-making method to come up with the most resilient network with multiple (or a single) microgrid(-s) for each operating scenario.

3.1. Constraints for microgrids formation in MILP

1 *Cluster formation constraints (CFC).* If the load at node $i \in N$ can be supplied by a distributed generator, this node can only belong to a certain microgrid m, while $m \in M$. However, some nodes may be not included to any MG due to DGs output limitations, and still being fed from the mains. Here the nodes, which are fed from the main grid, can be represented as a MG with a single source, while the power of this source should be equal (if no deficiency) to the difference between the load demand and the total power output of all operating DERs:

$$p_{source} = \partial_n \left(\sum_{i \in \overline{N}} p_i - \sum_{m \in M} p_m^{DG} \right), \ \forall\ i \in \overline{N}, \ m \in M, \tag{1}$$

$$q_{source} = \partial_n \left(\sum_{i \in \overline{N}} q_i - \sum_{m \in M} q_m^{DG} \right), \ \forall\ i \in \overline{N}, \ m \in M, \tag{2}$$

where ∂_n is the deficiency coefficient of the n-th operation scenario, which denotes the share of power, that can be taken from the main grid, with regard to power demand, $\partial_n \in [0, 1]$.

Besides, some loads may be isolated and de-energized in case of a HILP-caused fault. To model the cluster formation constraints, these nodes should be removed from N, which can be accomplished by finding the connected components of an undirected graph G of the PDS and removing the nodes and edges of the connected component without a power source.

Given that, the CFC can be written as

$$\sum_{m \in M} \alpha_{im} = 1, \ \forall\ i \in \overline{N}, \tag{3}$$

where $\alpha_{im} \in \{0, 1\}$ is the cluster formation constraint, which indicates the allegiance of the node $i \in \overline{N}$ to the MG $m \in M$, i.e. i belongs to m if $\alpha_{im} = 1$, and i does not belong to m otherwise.

Additional constraint should be expressed for the node i, which belongs to the MG m and has a DER:

$$\alpha_{im} = 1, \ i = m, \ \forall\ i \in \overline{N}, \ m \in M. \tag{4}$$

1 *Microgrid Connectivity Constraints (MCC).* A radial PDS can be exhibited as a tree of a connected graph $G(N, E)$ with the source node as the root. Similarly, MGs can be represented as subgraphs of the G with the DGs installed in the root nodes. Due to the connectivity trait of a tree [42], one node can belong to a MG m only if its parent node (i.e. for this MG) also belongs to the MG m, which can be expressed with inequality constraints [13]:

$$\alpha_{im} \leq \alpha_{jm}, \ \forall\ m \in M, \ i \in N \setminus \{m\}, \ j = \rho_m(i) \tag{5}$$

where $\rho_m(i)$ specifies the parent node of the node i with regard to the MG m.

1 *Microgrid Branch-Node Constraints (MBNC)* are considered with respect to the relation between nodes and branches in a MG and defined in [13]. In brief, if both nodes i and j belong to a microgrid m, i.e., $\alpha_{im} = \alpha_{jm} = 1$, then the branch between i and j should also belong to the MG m. Together with (5), it can be derived that if the children node of (i, j) (regarding the MG m) belongs to this MG, then the line (i, j) sits in the microgrid m. If the line (i, j) has a switch and belongs to any microgrid in M, the switch should be in the closed state. Therefore, the MBNC can be written as

$$\beta_{ij} = \sum_{m \in M} \alpha_{km}, k = c_m(i,j), \ (i,j) \in \overline{E}, \tag{6}$$

where $k = c_m(i, j)$ specifies the children node of the line (i, j), with regards to the MG m.

1 *Microgrid Load Pickup Constraints (MLPC)* are defined as per [13]. If the load at node i can be fed from a microgrid $m \in M$, the following two conditions should be satisfied:
- $\alpha_{im} = 1$, i.e., node i belongs to the MG m;
- $l_i = 1$, i.e., the load switch is closed.

These two conditions can be written as a quadratic constraint: $\alpha_{im} \cdot l_i = 1$.

To address this issue, define the auxiliary binary decision variables [13] $\gamma_{im} \in \{0, 1\}$ as $\gamma_{im} = \alpha_{im} \cdot l_i$, $\forall i \in \overline{N}$, $m \in M$, and the quadratic equality constraints can be further converted to the linear form:

$$\gamma_{im} \leq \alpha_{im}, \ \forall \ i \in \overline{N}, \ m \in M \tag{7}$$

$$\gamma_{im} \leq l_i, \ \forall \ i \in \overline{N}, \ m \in M \tag{8}$$

$$\gamma_{im} \geq \alpha_{im} + l_i - 1, \ \forall \ i \in \overline{N}, \ m \in M \tag{9}$$

3.2. Optimization task formulation

In a standard power distribution network loads have different importance of sustaining critical functions. In this paper all the loads are divided into three classes with regard to their priority:

- CLs: high priority loads, e.g., hospitals, fire stations, police departments;
- medium-critical loads (MCLs): medium priority loads, e.g., elementary and secondary schools, university departments, administration buildings;
- non-critical loads (NCLs): loads with low priority, e.g., residential and small commercial buildings.

Let w_i denote the priority weight associated with the load at a node i. Larger values of w_i correspond to higher priority. The objective of microgrids with dynamic boundaries formation is to pick up maximum loads, subject to the defined constraints, which can be expressed as a MILP problem

$$\max_{\alpha_{im}, \beta_{ij}, l_i, \gamma_{im}} \sum_{i \in \overline{N}} w_i \sum_{m \in M} \gamma_{im} \cdot p_i \tag{10}$$

subject to

$$\text{CFC}: \ (3), \ (4) \tag{11}$$

$$\text{MCC}: \ (5) \tag{12}$$

$$\text{MBNC}: \ (6) \tag{13}$$

$$\text{MLPC}: \ (7) - (9) \tag{14}$$

3.3. Power flow constraints

After the MG formation MILP problem is solved, the power flow calculation is to be performed to determine the node voltages and line currents at each point and branch of the PDS. In this paper a three-phase unbalanced Newton-Raphson method is employed to calculate the power flow. According to [43], first, the real current and imaginary current injections from loads into the system are to be calculated by the expressions:

$$\Delta I_{ri}^s = \frac{(P_i^{sp})^s V_{ri}^s + (Q_i^{sp})^s V_{mi}^s}{\left(V_{ri}^s\right)^2 + \left(V_{mi}^s\right)^2} - \sum_{k=1}^{n} \sum_t \left(G_{ik}^{st} V_{rk}^t - B_{ik}^{st} V_{mk}^t\right), \tag{15}$$

$$\Delta I_{mi}^s = \frac{(P_i^{sp})^s V_{mi}^s + (Q_i^{sp})^s V_{ri}^s}{\left(V_{ri}^s\right)^2 + \left(V_{mi}^s\right)^2} - \sum_{i=1}^{n} \sum_t \left(G_{ik}^{st} V_{mk}^t - B_{ik}^{st} V_{rk}^t\right), \tag{16}$$

where P_i is the real power component of a load in the node i; Q_i is the reactive power component of a load in the node i; V_{ri} is the real part of voltage; V_{mi} is the imaginary part of voltage, G_{ik} is the conductance of the k-th line; B_{ik} is the susceptance of the k-th line. The indices in (15), (16) denote the following: i is the node number, s is the current phase of interest, t states for all of the phases of the node.

When the current injections are obtained, the voltage updates are calculated via

$$\begin{bmatrix} \Delta I_{mi} \\ \Delta I_{ri} \end{bmatrix} = -J^{-1} \begin{bmatrix} \Delta V_{mi} \\ \Delta V_{ri} \end{bmatrix}, \tag{17}$$

where J^{-1} is the inverse Jacobian given by $J = \begin{bmatrix} \frac{\partial \Delta I_{mi}}{\partial V_{ri}} & \frac{\partial \Delta I_{mi}}{\partial V_{mi}} \\ \frac{\partial \Delta I_{ri}}{\partial V_{ri}} & \frac{\partial \Delta I_{ri}}{\partial V_{mi}} \end{bmatrix}$

The configuration of the PDS with MGs with flexible boundaries should satisfy operation constraints, namely power balance, voltage limit at each node, feeder current capacity limits [44,45].

Voltage limits constraints

$$\left|V_i^{\min}\right| \leq |V_i| \leq \left|V_i^{\max}\right| \tag{18}$$

Branch capacity constraints

$$\begin{aligned} |I_{Fi}| &\leq \left|I_{Fi}^{\max}\right| \\ |I_{Ri}| &\leq \left|I_{Ri}^{\max}\right| \end{aligned} \tag{19}$$

DG real and reactive power constraints

$$\begin{aligned} P_{DG}^{\min} &\leq P_{DG} \leq P_{DG}^{\max} \\ Q_{DG}^{\min} &\leq Q_{DG} \leq Q_{DG}^{\max} \end{aligned} \tag{20}$$

In the equations (18-20) V_i is the voltage in the i th node, I_{Fi} is the forward flow capacity of the i th distribution line; I_{Ri} is the reverse flow capacity of the i th distribution line; P_{DG} and Q_{DG} are the available real and reactive power capacities of the DGs. Superscripts min and max represent the maximum and minimum allowable limits of the corresponding values. Voltage deviations should not exceed ±0.1 p. u. violation threshold [46].

3.4. Resiliency-driven approach to form a PDS with multiple microgrids

After the MILP problem is solved and the constraints (18-20) are satisfied, the optimal architecture of a PDS with multiple (or single) MGs is determined for each operating scenario, and its resiliency performance is to be estimated. Besides, modification of MGs' boundaries through the activation/deactivation of the agents can be executed. Since

merging/splitting of networked MGs changes the topology of the PDS, it also impacts the resiliency, which should not be left unattended. In this paper eight resiliency metrics are picked up from [16,44], basing on their relevance and appropriateness for the current research objective. The first six metrics capture some key topological characteristics of the PDS, providing information about its efficiency, redundancy, robustness. The latter two metrics reflect the operational feasibility of the microgrids' configuration. A feasible microgrid (FMG) can be formed with a certain combination of switches, it is able to supply all the CLs, and complies with the radiality criteria and the operational constraints. In such a way, the selected set of metrics evaluates the power grid under study from the topological point of view, with respect to the graph theory, and from the performance point of view.

Definitions and mathematical expressions of the selected metrics are provided below.

1) The *diameter D* of a graph *G* is the maximum topological distance *d* (i.e. the number of edges) in the shortest path that connects the two most remote nodes [47]. It can be represented as

$$D = \max\left\{d\left(n_i, n_j\right) : \forall\left(n_i, n_j\right) \in N\right\}, \tag{21}$$

where n_i and n_j are nodes of the graph *G*.

Choosing a MG topology with a shorter diameter has several benefits: the risk of overloading is reduced, the closeness of reactive loads to reactive sources can contribute to the voltage profile improvement, and the power losses can be reduced due to shorter distances between sources and nodes [23].

2) *Aggregate Betweenness Centrality* (AC_B) is defined as the average difference of betweenness centrality between the most central vertex *n* of the graph, which has the highest value of betweenness, and all others [48]. For node n_i it can be calculated by

$$A_{..B}(n_i) = \frac{\sum_{n=1}^{N} \Omega_{n_i}^{q} \cdot \sum_{i \neq n \neq j} \frac{\sigma_{ij}(n_i)}{\sigma_{ij}}}{N}, \tag{22}$$

where σ_{ij} is the total number of shortest paths from node *i* to node *j*; $\sigma_{ij}(n_i)$ is the number of those paths through the node n_i; Ω_{ni}^{q} is the degree of node n_i in the *q*-th network configuration. The AC_B metric represents the concentration of the network topology around a central location.

3) *Algebraic Connectivity* λ_2 is the second smallest eigenvalue of a normalized Laplacian matrix (i.e., degree matrix minus adjacency matrix) of the network. It quantifies the network's structural robustness and fault tolerance [49].

$$\lambda_2 \ \leq \ n(G) \leq d_{\min}(G) \tag{23}$$

Larger values of λ_2 correspond to enhanced fault tolerance and robustness against network partition (i.e., against division into islands).

4) *Average path-length* l_q estimates the shortest distance *d* (i.e., the minimum number of branches) that need to be traversed in order to reach a node n_j from a node n_i [50]

$$l_q = \frac{1}{N(N-1)} \sum_{i,j} d(n_i, n_j) \tag{24}$$

This metric will provide a limited view of network reachability and efficiency in power distribution systems.

5) The *clustering coefficient* C_n of a certain topology of the graph *G* is defined as the average of the local clustering coefficients for all the nodes in *G* [47]

$$C_n = \frac{1}{N} \sum_{i \in N} \frac{y_i}{\binom{d_i}{2}}, \tag{25}$$

where y_i is the number of links between neighbors of n_i; d_i is the degree of the node n_i.

This value represents the probability that two neighbors of a node are neighbors themselves.

6) The *spectral radius* ρ is the largest absolute value among the eigenvalues of the adjacency matrix of the graph *G* [51]

$$\rho = \max_{1 \leq i \leq N} |\lambda_i| \tag{26}$$

The smaller the spectral radius, the higher the robustness of a network, and the better it is protected against cyber-attacks [52].

7) *Path Redundancy* (PR) is defined as the ratio of the total number of paths available for all CLs connecting to all sources to the total number of CLs in each FMG.

$$PR_{\mu} = \frac{Paths\ connecting\ all\ CLs\ to\ all\ sources\ in\ \mu - \text{th}\ FMG}{Number\ of\ CLs\ in\ \mu - \text{th}\ FMG} \tag{27}$$

8) *Possible Network Fraction* (PNF) is the number of possible networks with similar switch configurations, which can be combined in a single FMG.

$$PNF_{\mu} = \frac{PNs\ connecting\ all\ CLs\ to\ separate\ sources\ in\ \mu - \text{th}\ FMG}{Number\ of\ CLs\ in\ \mu - \text{th}\ FMG} \tag{28}$$

All the metrics are interdependent, and they change with the transformation of the network's configuration. The vector $\overrightarrow{\Re}_{\mu}$ provides a preliminary insight into the complex resiliency of each given feasible microgrid.

$$\overrightarrow{\Re}_{\mu} = \left[D,\ AC_B,\ \lambda_2,\ l_q,\ C_n,\ \rho,\ PR,\ PNF\right] \tag{29}$$

Obviously, not all metrics indicate resiliency equally good. Since unique numerical solutions are preferred for easier interpretation, the Analytic Hierarchy Process is a feasible approach to quantify resiliency based on the defined criteria. The process of resiliency estimation using AHP implies assigning weights to the network metrics. Then the method organizes the criteria in a hierarchical manner to satisfy the multi-criteria analysis. For the analyzed set of criteria, defined by the vector $\overrightarrow{\Re}_{\mu}$ as per (29), the result of the pairwise comparison can be summarized in a $k \times k$ matrix *K*, where the element ε_{ij} ($i, j = 1, 2, ..., k$) indicates the relative importance of a criteria *i* with respect to a criteria *j* [53]:

$$K = \begin{bmatrix} \varepsilon_{11} & \varepsilon_{12} & \cdots & \varepsilon_{1k} \\ \varepsilon_{21} & \varepsilon_{22} & \cdots & \varepsilon_{2k} \\ \vdots & \vdots & \ddots & \vdots \\ \varepsilon_{k1} & \varepsilon_{k2} & \cdots & \varepsilon_{kk} \end{bmatrix}, \ \varepsilon_{ii} = 1, \ \varepsilon_{ji} = \frac{1}{\varepsilon_{ij}}, \ \varepsilon_{ij} \neq 0 \tag{30}$$

Next the geometric means of each row are to be calculated by

$$\left(\prod_{i=1}^{k} \varepsilon_i\right)^{\frac{1}{k}} = \sqrt[k]{\varepsilon_{11}\varepsilon_{12}...\varepsilon_{1k}} \tag{31}$$

And the relative normalized weight (W_i) of each criteria can be obtained [54].

$$W_i = \frac{\left(\prod_{i=1}^{k} \varepsilon_i\right)^{1/k}}{\sum_{j=1}^{j=k} \left(\prod_{i=1}^{k} \varepsilon_i\right)^{1/k}} \tag{32}$$

Determining the weights can be considered as a problem of solving a matrix equation with matrix of columns *W* solution for eigenvalues λ different from 0 [53].

$$\Re_{\mu} = K \times W = \begin{bmatrix} 1 & \varepsilon_{12} & \cdots & \varepsilon_{1k} \\ \varepsilon_{21} & 1 & \cdots & \varepsilon_{2k} \\ \vdots & \vdots & \ddots & \vdots \\ \varepsilon_{k1} & \varepsilon_{k2} & \cdots & 1 \end{bmatrix} \times \begin{bmatrix} W_1 \\ W_2 \\ \cdots \\ W_k \end{bmatrix} = \begin{bmatrix} \lambda_1 W_1 \\ \lambda_2 W_2 \\ \cdots \\ \lambda_k W_k \end{bmatrix} \tag{33}$$

The maximum eigenvalue λ_{max} in (33) will correspond to the highest

priority. The criteria are compared pairwise and based on a semantic Saaty scale [55], which is user-defined to indicate the dominance of one particular metric over others. The pairwise comparison was then checked for consistency to ensure that the user-defined comparisons provide proper results. An inconsistency of 10% is tolerated in AHP.

If during a certain operational scenario the PDS is composed of m microgrids, a vector of composite resiliency can be written for each q-th network configuration:

$$\Re_q^{config} = \left[\Re_{\mu_1},\ \Re_{\mu_2}, \ldots,\ \Re_{\mu_m}\right] \tag{34}$$

The composite resiliency for the whole PDS with multiple microgrids can be expressed as

$$\Re_q^{config} = \Re_\mu^{\max} + \left(1 - \Re_\mu^{\max}\right) \sum_{q=1}^{n-1} \left(\frac{\Re_{\mu_m} \vartheta_q \sum_{i=1}^{N^{\mu_m}} w_i p_i}{\sum_{m=1}^{M} \sum_{i=1}^{N^{\mu_m}} w_i p_i} \right), \tag{35}$$

where $\Re_\mu^{\max}$ corresponds to the MG with the highest composite resiliency value; $\Re_{\mu_m}$ is the resiliency value of the m-th MG, which is lower than the maximum one; ϑ_q is the normalized weight assigned to the resiliency metrics $\Re_{\mu_m}$ of the q-th MG. Subscript μ_m denotes the belongingness to m-th MG. Values ϑ_q must be assigned to resiliency metrics of the MGs in a descending order and, obviously, their sum must be less than 1 in order to obtain a non-distorted result that obeys the inequality $0 \le \Re_q^{config} \le 1$.

In this paper, the normalized weights were calculated on the basis of a geometric progression so that

$$\vartheta_q = \vartheta_1 U^{q-1}, \tag{36}$$

where $\vartheta_1 = 1$ is the normalized weight of $\Re_\mu^{\max}$, U is the descending coefficient, which is user-defined.

3.5. Proposed algorithm

The flowchart of the proposed resiliency-based algorithm for formation of self-adequate MGs with flexible boundaries is depicted in Fig. 1.

The algorithm starts with the first stage, which is the MGs formation problem. To obtain the operationally feasible multi-microgrid PDS it is necessary to determine the load composition and available power sources for each operational scenario (e.g., different loadings for daytime and nighttime, for a working day and a weekend, for different seasons), and to assign priority weights to CLs, MCLs, and NCLs. The CLs have the highest priority and should not be lost. Secondly, mixed integer programming is to be applied to form MGs, and the MILP constraints are to be checked. If it is possible to squeeze or to enhance the microgrids' boundaries to adapt to different loading scenarios, then PDS with flexible boundaries can be created. The number of network configurations (i.e., power networks with unique MGs) corresponds to the number of

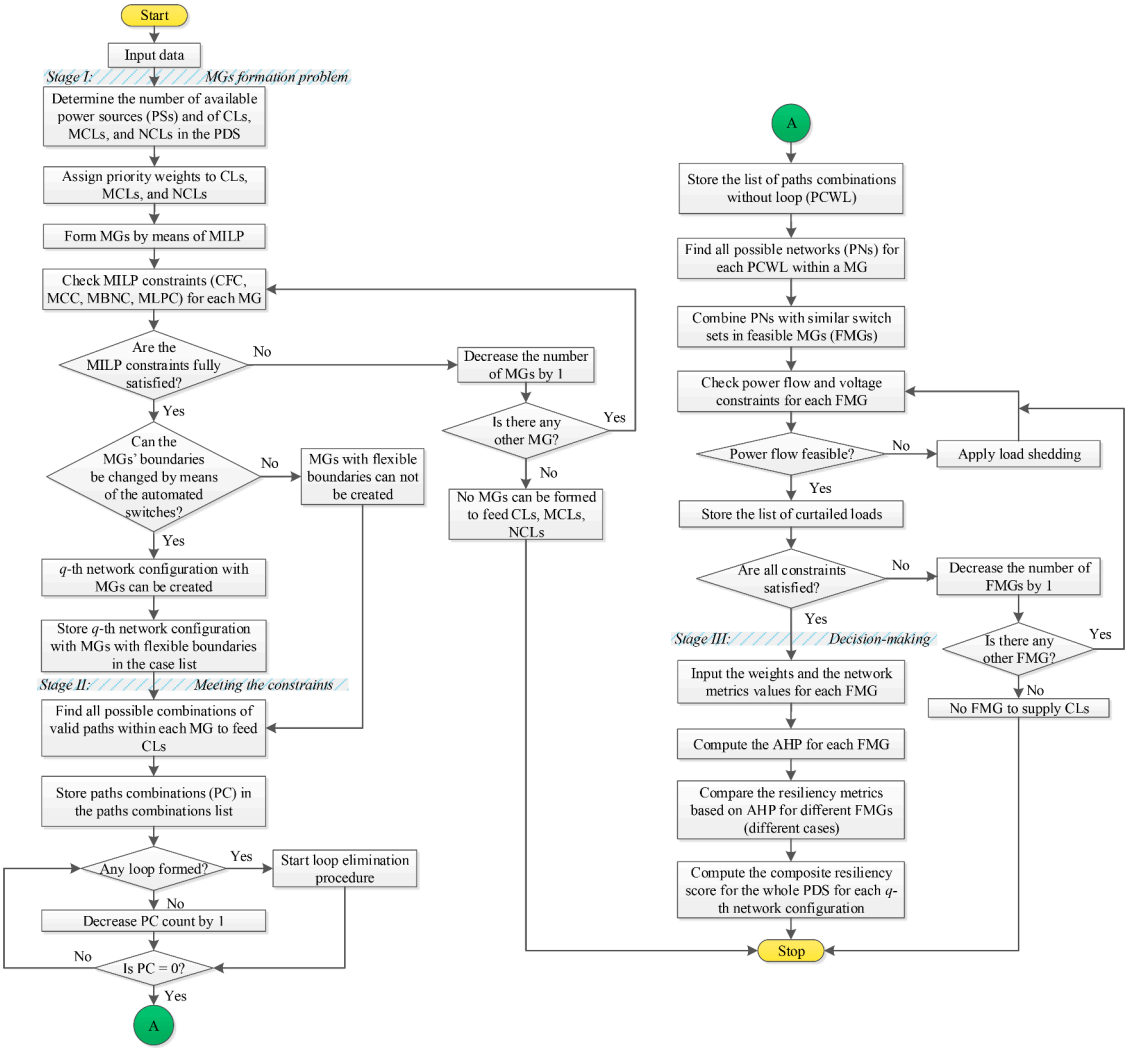

Fig. 1. Algorithm to enable operational resiliency using MGs with flexible boundaries.

feasible microgrids with different boundaries. The boundary adjustments are to be coordinated by means of the automated switches. The next stage begins with finding all possible paths connecting critical loads and power sources within each MG. To maintain the radial nature of MGs, the paths containing loops must be excluded using the loop elimination technique [44]. Next, possible network configurations without loops (PCWL) and with similar switch statuses, which can be formed within a single MG, are combined in sets. Each set corresponds to a unique feasible microgrid. Further, the power flow calculations are to be made in GridLAB-D and, independently, in MATLAB. The power flow convergence in GridLAB-D and MATLAB and cohesion of the results obtained is considered as proof of correctness. At this point, there is a repeating loop, meaning that until the power flow is converged, the load is reduced, and the power flow is recalculated. There are several methods for identifying sensitive loads and performing load curtailment [56,57]. However, this is out of the scope of this study, and for simplicity at each iteration the load with the smallest active power value and the lowest priority weight is shed. Feasible networks, which satisfy all the operation constraints, are to be stored, and the resiliency quantification is to be calculated for each FMG at the third stage. Eventually, the composite resiliency metric for the q-th PDS's configuration is to be calculated.

Alternative flexible boundaries of the MG must be preplanned and dynamically changed during operation (prior to a HILP event or, otherwise, afterwards). Thus, the proposed composite method contains both planning and operational decision-making. The first stage of the algorithm, which is the MGs formation problem, should be executed beforehand, during the planning decision-making. When the operation conditions change normally (e.g., daily, weekly, and seasonal load flow variations, which can be predicted in advance with a certain tolerance), the second and the third stages of the algorithm, which are checking the constraints and obtaining the composite resiliency score, should be done in a planning manner. However, for emergency conditions, the information about the possible combinations of valid paths within each MG to CLs needs to be updated, which means that the second and the third stages shift to the operational decision-making domain.

4. Case study

4.1. Resiliency-driven determination of MGs' boundaries

The modified IEEE 123 node test feeder [44] (Fig. 2) is exploited to demonstrate the effectiveness of the proposed approach. The feeder has 122 branches, with sectionalizers in each one, and 12 tie-line switches. It is assumed that all the loads are switchable. TOMLAB/AMPL v2.0 (GUROBI v5.6) Optimization Environment is exploited to solve the MILP problem of MG formation. MATLAB 2018b is used to formulate the model and link the TOMLAB solver. The simulations were done using a CPU with the following specifications: Intel® Core i7–8550 processor, 1.80 GHz, 64 bit, and 8 GB RAM. Four DERs and two energy storages are available and connected at buses 21, 49, 50, 72, 76, 105. The information of the injected DGs, including photovoltaic (PV) arrays, wind turbines (WTs), and energy storage (ES) is listed in Table 1.

Loads are divided into three classes, as described in Section 3.2, and the weighting factors for CLs, MCLs, and NCLs are 100, 10, and 0.1, respectively. Load classes and the deployed DGs are marked distinctively in Fig. 2. Two operating scenarios are considered, represented by the average power demand (load demand) for daytime and for nighttime. It is assumed that after sunset the power consumption in the PDS drops to 40% from the day value. During the daytime, all the DERs continuously operate at their rated power ratings, and ESs soak up the power surplus, released by the PV arrays and the WTs. During the nighttime, the PV arrays do not produce power, and the loads are fed by the ESs and the WTs.

The elaborated method is applied to determine the optimal number of MGs and define their boundaries. At the first stage the MILP MGs formation problem is solved. In this paper the only considered case for normal operation is when all the loads are supplied without any curtailment, i.e., 100% of load demand is satisfied. At the next stage the power flow constraints are checked for satisfaction, and non-feasible network configurations are eliminated. For the daytime operation the configuration with four MGs and a grid-connected part (Fig. 3) is obtained, and for the nighttime operation the configuration with two MGs and a grid-connected part (Fig. 4) is identified.

At the third stage of the proposed method, the resiliency-driven decision about the final network configuration is to be made. The islands circled with dotted lines in Fig. 3 and in Fig. 4 can be further connected

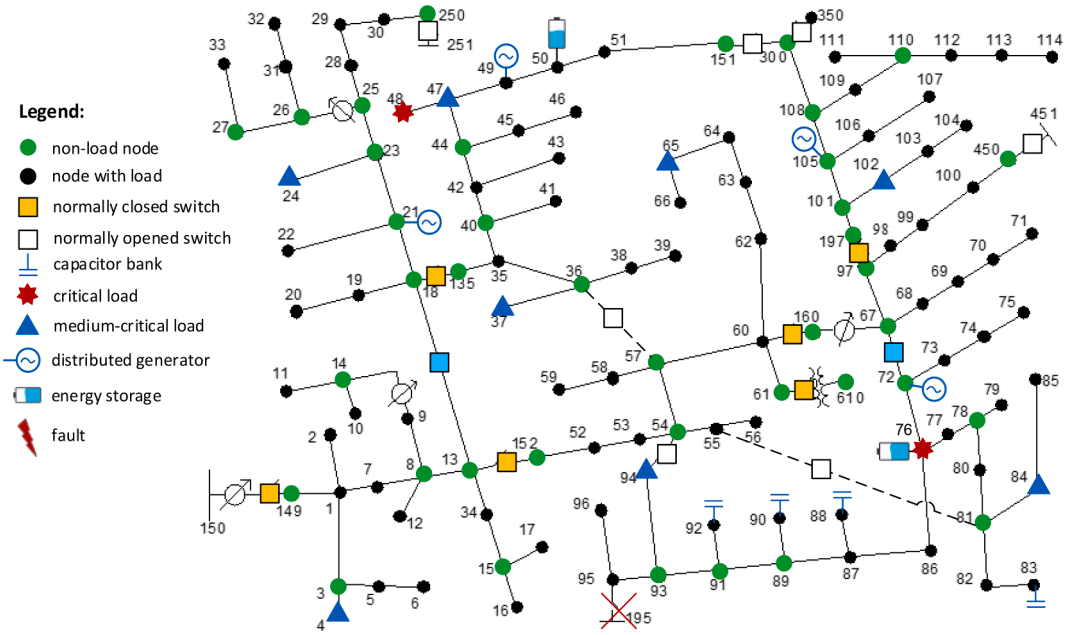

Fig. 2. One-line diagram of the modified IEEE 123 node test feeder.

Table 1
Distributed generators and electric storage data.

DER No	Node No	DER type	cosφ	Power ratings for phases A-C					
				P_A, kW	Q_A, kvar	P_B, kW	Q_B, kvar	P_C, kW	Q_C, kvar
1	21	PV	0.89	200	100	40	20	120	60
2	49	PV	0.85	300	180	255	165	200	125
3	50	ES	0.85	180	102	86	58	84	52
4	72	PV	0.87	265	160	290	160	310	170
5	76	ES	0.87	106	64	116	64	124	68
6	105	WT	0.89	140	70	80	40	100	50

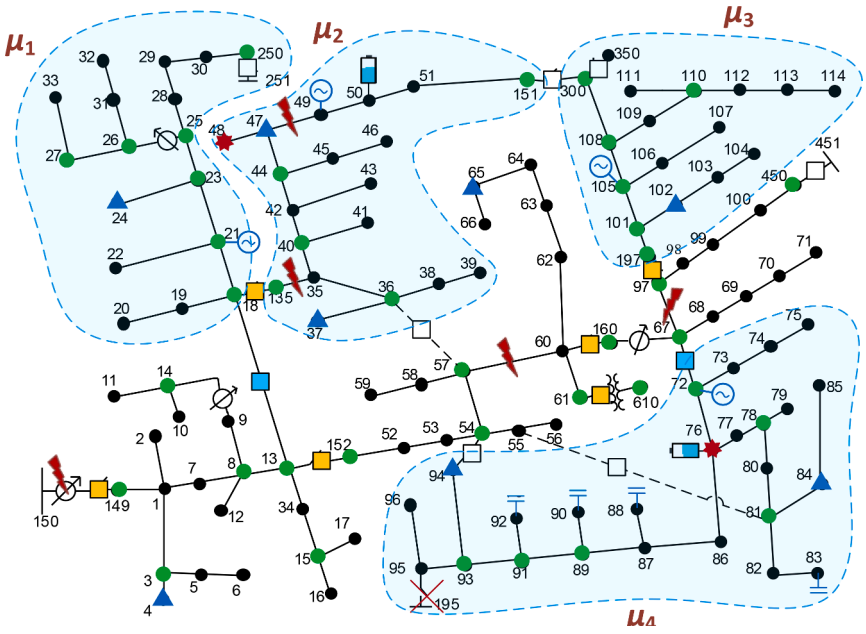

Fig. 3. The topology of the studied PDS for daytime operation (4 MGs).

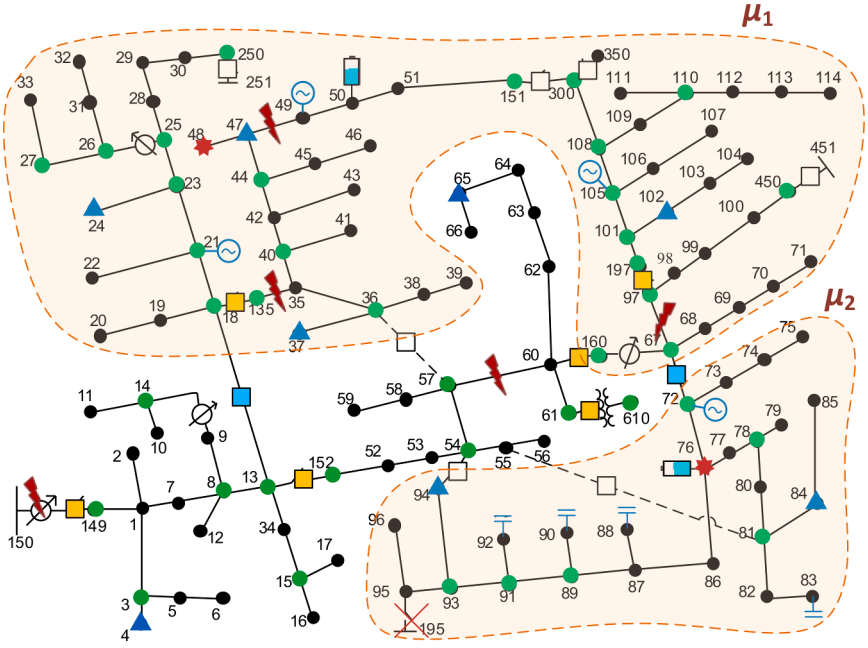

Fig. 4. The topology of the studied PDS for the nighttime operation (2 MGs).

Table 2
Switch status for different feasible configurations of the PDS.

Switch status	Normally CLOSED								Normally OPENED			
No	13-18	13-152	18-135	60-160	61-610	97-197	150-149	67-72	54-94	151-300	36-57	55-81
Case	Switch status for saving CLs and MCLs											
MG1, MG2, MG3, MG4	0	1	0	1	1	0	1	0	0	0	0	0
Merged MGs1,2 & MG3, MG4	0	1	1	1	1	0	1	0	0	0	0	0
Merged MGs2,3 & MG1, MG4	0	1	0	1	1	0	1	0	0	1	0	0
Merged MGs1,2,3 & MG4	0	1	1	1	1	0	1	0	0	1	0	0
MG1, MG2	0	1	1	1	1	1	1	0	0	1	0	0
Merged MGs1,2	0	1	1	1	1	1	1	1	0	1	0	0
Contingency, day	1	0	0	1	1	1	0	1	0	1	1	1
Contingency, night	0	1	0	1	1	1	0	1	0	1	1	1

Table 3
Resiliency metrics for MGs.

Period	Microgrid	D	AC_B	λ_2	l_q	C_n	ρ	PR_μ	PNF_μ
Day	Grid-connected part, day	20	0.75	0.0102	8.4586	1.4843	5.5809	0.5	0.5
	MG1	9	0.93	0.0745	4.2810	1.4444	4.9455	1	1
	MG2	11	0.96	0.0522	4.4632	1.3	5.1281	2	1.3333
	MG3	10	0.99	0.0699	4.05	1.375	4.947	1	1
	MG4	13	0.96	0.0328	5.6067	1.36	5.0003	2	1.3333
	Merged MGs1,2	17	0.86	0.0179	6.8348	1.3514	5.1560	3	2.25
	Merged MGs2,3	18	0.93	0.0141	7.6540	1.3889	5.1281	3	2.25
	Merged MGs1,2,3	24	0.87	0.0075	9.8737	1.3962	5.1560	4	3.2
Night	Grid-connected part, night	17	0.81	0.0161	7.1474	1.4333	5.5809	0.5	0.5
	MG1	28	0.82	0.0053	11.2538	1.4256	5.3805	2	1.6
	MG2	13	0.96	0.0328	5.6067	1.36	5.0003	1	0.6667
	Merged MGs1,2	34	0.73	0.0033	13.4919	1.4074	5.4581	3	2.25

by closing the automated switches between them. This will allow coordination of multiple sources, including MGs and different types of DGs, to mitigate superior uncertainty management of renewable energy sources [23]. For the daytime operation four MGs formation cases are possible: 1) all the four MGs operate in the islanded mode; 2) MG μ_1 and MG μ_2 are merged, while MGs μ_3 and μ_4 operate independently; 3) MG μ_2 and MG μ_3 are merged, while MGs μ_1 and μ_4 operate independently; 4) MG μ_1, MG μ_2, and MG μ_3 are merged, while MGs μ_4 operates independently. For the nighttime operation two MGs formation scenarios are possible: 1) both MG μ_1 and MG μ_2 are in the islanded mode; 2) MG μ_1 and MG μ_2 are merged. The unique network configurations with corresponding switch statuses for these cases are shown in Table 2. The 0 indicates the normally opened switch, while the 1 indicates the normally closed switch.

To find the most resilient configuration, the resiliency metrics for each scenario (4 scenarios for the daytime and 2 scenarios for the nighttime operation) are to be assessed. Results of the resiliency metrics computation for different MGs are listed in Table 3. The network fraction, which is fed from the mains, is treated as a MG, as was explained in Section 2.

Next, it is necessary to calculate the factor-based resiliency metric for each FMG. For this purpose, the 8 × 8 pairwise comparison matrix (Table 4) was assigned to all the feasible topologies. The inputs are to be subjectively determined by users (e.g., DSOs), basing on their experience and awareness about the system's state. All the eight criteria defined in Section 3.4, D are compared pairwise with respect to the objective, which is to maximize the resiliency of the power distribution system and to save maximum loads.

During calculations it is essential to take into account that some network parameters contribute to strengthening the resiliency, while others decrease it. The influence of the network indicators on resiliency performance is shown in Table 5. For higher $\Re_\mu$ indicators with negative impact should be reduced, while indicators with positive impact should be magnified.

The AHP values were obtained using input values and pairwise comparative weights. The degrees of interaction are identified by the significance ratio between maximum and minimum input values of the network metrics. The AHP pairwise comparison matrix has an inconsistency of 2.88%, which satisfies the defined 10% inconsistency threshold. The calculated results are shown in Table 6. The integrated resiliency metric of the whole PDS of a given configuration is calculated by (35). In (36) the descending coefficient is assumed 0.518 for daytime and 0.618 for nighttime. The results of Table 6 show that the PDS has the highest resiliency $\Re_q^{config}$, when all the possible microgrids are in the

Table 4
Pairwise comparison matrix with weight coefficients for topology-based metrics.

Criteria	D	AC_B	λ_2	l_q	C_n	ρ	PR	PNF	Weights
D	1	2	1	1	6	1	1.5	1.5	**0.1674**
AC_B	0.5	1	0.5	1.5	2	0.5	1	1	**0.1054**
λ_2	1	2	1	1	5	1.5	2	1.75	**0.1805**
l_q	1	0.667	1	1	3	1	3.5	2.5	**0.1708**
C_n	0.167	0.5	0.2	0.333	1	0.25	0.333	0.333	**0.0376**
ρ	1	2	0.667	1	4	1	1.5	1.5	**0.1511**
PR	0.667	1	0.5	0.286	3	0.667	1	1.25	**0.0942**
PNF	0.667	1	0.571	0.4	3	0.667	0.8	1	**0.093**

Table 5
The influence of the network-based factors on resiliency.

Influence	Resiliency metrics							
	D	AC_B	λ_2	l_q	C_n	ρ	PR	PNF
Positive			•		•		•	•
Negative	•	•		•		•		

islanded mode, as shown in Fig. 3 and in Fig. 4. Note that this result can be changed if different weights are assigned to the resiliency metrics during AHP pairwise comparison. Thus, the resiliency performance depends on the priority of the used metrics, which can be adjusted by a DSO or by a power system engineer with respect to the peculiarities of the maintained PDS.

According to the composite resiliency scores from Table 6, a DSO (or automatics) should set the most appropriate operational modes as follows.

- For the daytime it is suggested that the multi-microgrid PDS operates under the first scenario, when all the four MGs are in the islanded mode. In this case, the resiliency performance of the system is about 8% better, compared to the least desired scenario with merged MGs μ_1, μ_2, μ_3 and islanded MG μ_4.
- For the nighttime it is suggested that the multi-microgrid PDS operates with both MG μ_1 and MG μ_2 in the islanded mode. This configuration is 1.24 times more resilient, compared to the configuration with merged MG μ_1 and MG μ_2.

The switches' statuses for the aforementioned configurations are listed in Table 2.

4.2. Contingency scenario

In this subsection the efficiency of the proposed algorithm in restoration of the disrupted service is assessed. A contingency scenario has been formulated for the modified IEEE 123 node test system Fig. 2. For the further considered scenario it is assumed, that when a fault or a hazardous event occurs, the protection system isolates the faulted/damaged area. Five faults occur due to a hazardous event (e.g., a hurricane), and the corresponding faulted lines are 47–49, 57–60, 67–97, 135–35, and 150–149, which are marked with the "lighting" signs in Fig. 3 and Fig. 4. The faulted sections will be automatically isolated from the rest of the PDS by sectionalizers.

First, consider the situation when the contingency happens at the daytime. For the changed topology the MILP algorithm proposes to create two MGs, the first with nodes 1–34, 250, and the second with the rest of the nodes. The switch statuses for this contingency are shown in Table 2. The DER in the node 21 will supply MCLs 4 and 24, the DER and the ES in the nodes 72 and 76 will pick up the CLs 48, 76 and the MCLs 37, 47, 65, 84, 94, the DERs in the nodes 49 and 105 will feed the loads 49–51, 98–114, including the MCL 102. In order to comply with the power flow constraints, some NCLs must be curtailed, namely the loads 1–17, 30, 34, 52–64, 66. The objective of formation of microgrids with dynamic boundaries to pick up maximum loads, defined by (10), is satisfied at 99.958%. None of the CLs or MCLs are lost. On the contrary, the restoration strategy with static MGs with predefined boundaries

Table 6
Resiliency performance of the PDS with multiple MGs of different boundaries.

Time period	Case	Grid-connected part	MG1	MG2	MG3	MG4	Merged MGs1,2	Merged MGs2,3	Merged MGs1,2,3	$\Re_q^{config}$
		MG resiliency metrics $\Re_\mu$								
Day	MG1, MG2, MG3, MG4	0.2365	0.7514	0.6167	0.6920	0.5523	–	–	–	0.3842
	Merged MGs1,2 & MG3, MG4	0.2365	–	–	0.6920	0.5523	0.493	–	–	0.3646
	Merged MGs2,3 & MG1, MG4	0.2365	0.7514	–	–	0.5523	–	0.4303	–	0.363
	Merged MGs1,2,3 & MG4	0.2365	–	–	–	0.5523	–	–	0.3627	0.3545
Night	MG1, MG2	0.4569	0.3737	0.6975	–	–	–	–	–	0.425
	Merged MG1,2	0.4569	–	–	–	–	0.3488	–	–	0.343

does not allow MGs interconnection, and in this case the CL 48 and the MCLs 4, 37, 47, and 65 would be unsupplied.

Next, consider the situation when a similar contingency happens at night. The switch positions are shown in Table 2. For the changed topology the MILP algorithm proposes to form a single large island, which allows the coordination of multiple sources for service restoration. The ES in the node 76 will feed the CLs 48, 76, the MCLs 37, 47, 65, 84, and the NCL 77. ES in the node 50 and the DER in the node 105 will feed the MCL 102 and the NCLs 49–51, 98–114. The MCL 94 and the rest of the NCLs are curtailed to comply with the power flow constraints. The objective to pick up maximum loads is satisfied at 98.988%. In case of the traditional MGs with fixed boundaries, the CL 48 and the MCLs 4, 24, 37, 47, and 65 would be de-energized.

In such a way, formation of MGs with flexible boundaries helps to improve the resiliency performance of the PDS and to save important community loads, which would be inevitably lost in case of a traditional PDS architecture with MGs with fixed boundaries. The proposed approach allows to preliminary plan the alternative flexible boundaries of the MGs, basing on the comparison of the complex resiliency scores of each given FMG. For the studied example, the MGs with dynamic boundaries demonstrated self-healing capability to recover from faults during contingency scenarios, and all the CLs were saved. However, some of the less-priority loads could not be picked up due to the lack of resources. Therefore, system planners may consider implementing infrastructure-hardening strategies to enhance the PDS's robustness and resistance to the impacts of disastrous events and to smoothen the recovery process. Additionally, a forecast of the upcoming HILP event could provide information necessary to identify possible vulnerable areas, prepare DERs, and proactively realign to the most resilient configuration of the multi-microgrid PDS.

5. Conclusions

In this paper, the resiliency-driven algorithm to formulate adaptive self-adequate microgrids with flexible boundaries has been developed. The changing boundaries of the MGs are to be preplanned, and transition to the most resilient configuration can be made in advance, prior to the anticipated HILP event (planning decision-making), or afterwards, during the service restoration stage (operational decision-making). The mixed-integer linear programming is employed to determine switching actions to optimally reconfigure microgrids and maximize supply to critical loads while meeting all the system constraints. Two different operating scenarios are considered – for daytime and for nighttime. Also, DERs of various natures are deployed in the PDS to add the variety of possible constraints for flexible boundary scenarios.

The MILP-based three-stage formulation is applied to estimate the optimal numbers of MGs and define their boundaries. In the first stage, the MGs formation problem is solved. The second stage ensures meeting of the power flow constraints. The third stage provides a resiliency-driven decision to enable the most resilient networked microgrids with dynamic frontiers. The possibility of networked MGs and multiple sources coordination is considered, and the resiliency-driven decision about the final network configuration is obtained. The composite resiliency score for each feasible network topology is derived from eight different resiliency metrics via Analytical Hierarchy Process.

The effectiveness of the developed method to enable resiliency against probable contingencies and adverse natural events was demonstrated on the modified IEEE 123 bus system with MGs. In contrast to the conventional MGs with static boundaries, the MGs with flexible boundaries are more adaptable to various outages and HILP scenarios and outstand in terms of resiliency performance. The proposed algorithm can provide DSOs and system planning engineers with insights into the most resilient configuration with MGs for high-priority CLs serving. Therefore, it can be utilized in power system planning, operation, and decision-making to enhance operational resiliency and invest in system upgrades appropriately.

For future work it is planned to employ stochastic programming to capture the uncertainty and weather dependence of non-dispatchable dispersed generation, such as PV and wind generation units, which can help to better match the generation and demand of the PDS during the restoration process.

CRediT authorship contribution statement

Illia M. Diahovchenko: Methodology, Investigation, Validation, Resources, Data curation, Visualization, Software, Writing – original draft, Writing – review & editing. **Gowtham Kandaperumal:** Investigation. **Anurag K. Srivastava:** Conceptualization, Writing – review & editing.

Declaration of Competing Interest

The authors declare that they have no known competing financial interests or personal relationships that could have appeared to influence the work reported in this paper.

Data availability

Data will be made available on request.

Acknowledgements

The authors thank Fulbright Program in Ukraine, Institute of International Education, and the United States Department of Energy for making possible the research behind this paper.

References

[1] "Hurricane Costs," National Oceanic and Atmospheric Administration. [Online]. Available: https://coast.noaa.gov/.
[2] T. Ding, Y. Lin, Z. Bie, C. Chen, A resilient microgrid formation strategy for load restoration considering master-slave distributed generators and topology reconfiguration, Appl. Energy 199 (2017) 205–216.
[3] G. Liang, S.R. Weller, J. Zhao, F. Luo, Z.Y. Dong, The 2015 Ukraine blackout: implications for false data injection attacks, IEEE Trans. Power Syst. (2017).
[4] R. Dube, C. Maolis, Venezuela blackout plunges millions into darkness, Wall Street J. (2019) [Online]. Available: https://www.wsj.com/ [Accessed: 22-Mar-2019].
[5] N. Lin, The Timeline and Events of the February 2021 Texas Electric Grid Blackouts, Austin, 2021.
[6] N. Schifrin, "Russian attacks on energy infrastructure leaves Ukraine in dark as winter approaches," 2022. [Online]. Available: https://www.pbs.org/newshour/show/russian-attacks-on-energy-infrastructure-leaves-ukraine-in-dark-as-winter-approaches.
[7] I. Nikolaieva, W. Zwijnenburg, "Risks and impacts from attacks on energy infrastructure in Ukraine," 2022.
[8] Executive Office of the President of the United States, "Economic benefits of increasing electric grid resilience to weather outages," 2013.
[9] H.R. Esmaeilian, R. Fadaeinedjad, Energy loss minimization in distribution systems utilizing an enhanced reconfiguration method integrating distributed generation, IEEE Syst. J. (2015).
[10] M.W. Siti, D.V. Nicolae, A.A. Jimoh, A. Ukil, Reconfiguration and load balancing in the LV and MV distribution networks for optimal performance, IEEE Trans. Power Deliv. (2007).
[11] C. Lee, C. Liu, S. Mehrotra, Z. Bie, Robust distribution network reconfiguration, IEEE Trans. Smart Grid (2015).
[12] X. Chen, W. Wu, B. Zhang, Robust restoration method for active distribution networks, IEEE Trans. Power Syst. (2016).
[13] C. Chen, J. Wang, F. Qiu, D. Zhao, Resilient distribution system by microgrids formation after natural disasters, IEEE Trans. Smart Grid (2016).
[14] DOE, Summary report: 2012 DOE Microgrid Workshop, U.S. Dep. Energy, 2012, pp. 1–33.
[15] A. Hirsch, Y. Parag, J. Guerrero, Microgrids: a review of technologies, key drivers, and outstanding issues, Renew. Sustain. Energy Rev. (2018).
[16] I. Diahovchenko, G. Kandaperumal, A.K. Srivastava, Distribution power system resiliency improvement using distributed generation and automated switching, in: 2019 IEEE 6th International Conference on Energy Smart Systems, IEEE ESS, 2019.
[17] S.P. Burger, J.D. Jenkins, S.C. Huntington, I.J. Pérez-Arriaga, Why distributed? IEEE Power Energy Mag. 17 (2) (2019) 16–24.
[18] O. Rubanenko, O. Miroshnyk, S. Shevchenko, V. Yanovych, D. Danylchenko, and O. Rubanenko, "Distribution of wind power generation dependently of

meteorological factors," in *2020 IEEE KhPI Week on Advanced Technology, KhPI Week 2020 - Conference Proceedings*, 2020.
[19] I. Diahovchenko and Z. Viacheslav, "Optimal composition of alternative energy sources to minimize power losses and maximize profits in distribution power network," in *2020 IEEE 7th International Conference on Energy Smart Systems, ESS 2020 - Proceedings*, 2020.
[20] Institute of Electrical and Electronics Engineers, IEEE Std 1547.4™-2011, IEEE Stand. Coord. Comm. 21 (2011).
[21] M. Khederzadeh, S. Zandi, Enhancement of distribution system restoration capability in single/multiple faults by using microgrids as a resiliency resource, IEEE Syst. J. (2019).
[22] F. Shariatzadeh, N. Kumar, A.K. Srivastava, Optimal control algorithms for reconfiguration of shipboard microgrid distribution system using intelligent techniques, IEEE Trans. Ind. Appl. (2017).
[23] Y. Wang, et al., Coordinating multiple sources for service restoration to enhance resilience of distribution systems, IEEE Trans. Smart Grid (2018) 1, vol. PP, no. c.
[24] B. Chen, Z. Ye, C. Chen, J. Wang, T. Ding, Z. Bie, Toward a synthetic model for distribution system restoration and crew dispatch, IEEE Trans. Power Syst. (2019).
[25] S. Cai, Y. Xie, Q. Wu, Z. Xiang, X. Jin, M. Zhang, Robust coordination of multiple power sources for sequential service restoration of distribution systems, Int. J. Electr. Power Energy Syst. (2021).
[26] G. Kandaperumal, S. Pandey, A.K. Srivastava. Enabling electric distribution system resiliency through metrics-driven black start restoration, *IEEE Industry Applications Society*, 2021.
[27] A. Younesi, H. Shayeghi, A. Safari, P. Siano, Assessing the resilience of multi microgrid based widespread power systems against natural disasters using Monte Carlo Simulation, Energy (2020).
[28] V. Venkataramanan, A. Hahn, A. Srivastava, Cyphyr: a cyber-physical analysis tool for measuring and enabling resiliency in microgrids, IET Cyber-Physical Syst. Theory Appl. (2019).
[29] M. Borghei, M. Ghassemi, Optimal planning of microgrids for resilient distribution networks, Int. J. Electr. Power Energy Syst. (2021).
[30] B. Chen, J. Wang, X. Lu, C. Chen, S. Zhao, Networked microgrids for grid resilience, robustness, and efficiency: a review, IEEE Trans. Smart Grid (2021).
[31] A. Barnes, H. Nagarajan, E. Yamangil, R. Bent, S. Backhaus, Resilient design of large-scale distribution feeders with networked microgrids, Electr. Power Syst. Res. (2019).
[32] S.Y. Shevchenko, V.V. Volokhin, I.M. Diahovchenko, Power quality issues in smart grids with photovoltaic power stations, Energetika 63 (4) (2017).
[33] A. Hussain, A. Oulis Rousis, I. Konstantelos, G. Strbac, J. Jeon, H.M. Kim, Impact of uncertainties on resilient operation of microgrids: a data-driven approach, IEEE Access (2019).
[34] M.E. Nassar, M.M.A. Salama, Adaptive self-adequate microgrids using dynamic boundaries, IEEE Trans. Smart Grid (2016).
[35] H.H.Z. Mahdi Debouza, Ahmed Al-Durra, Tarek H.M. EL-Fouly, Survey on microgrids with flexible boundaries: strategies, applications, and future trends, Electr. Power Syst. Res. 205 (107765) (2022).
[36] Y.J. Kim, J. Wang, X. Lu, A framework for load service restoration using dynamic change in boundaries of advanced microgrids with synchronous-machine DGs, IEEE Trans. Smart Grid (2018).
[37] Y. Ma, et al., Real-time control and operation for a flexible microgrid with dynamic boundary, in: 2018 IEEE Energy Conversion Congress and Exposition, ECCE, 2018, p. 2018.
[38] S. Zhen, Y. Ma, F. Wang, L.M. Tolbert, Operation of a flexible dynamic boundary microgrid with multiple islands, in: Conference Proceedings - IEEE Applied Power Electronics Conference and Exposition, APEC, 2019.
[39] H.A. Abdelsalam, A. Eldosouky, A.K. Srivastava, Enhancing distribution system resiliency with microgrids formation using weighted average consensus, Int. J. Electr. Power Energy Syst. 141 (Oct. 2022), 108161.
[40] Y. Du, X. Lu, H. Tu, J. Wang, S. Lukic, Dynamic microgrids with self-organized grid-forming inverters in unbalanced distribution feeders, IEEE J. Emerg. Sel. Top. Power Electron. (2020).
[41] S. Konar, A.K. Srivastava, Look-ahead corrective restoration for microgrids with flexible boundary, in: In 2021 North American Power Symposium (NAPS), 2021, pp. 1–6.
[42] J. a Bondy, U.S.R. Murty, Graph Theory With Applications - J. Bondy, U. Murty. pdf, Oper. Res. Q. (1976), 19701977.
[43] P.A.N. Garcia, J.L.R. Pereira, S. Carneiro, V.M. Da Costa, Three-phase power flow calculations using the current injection method, IEEE Trans. Power Syst. (2000).
[44] I.M. Diahovchenko, G. Kandaperumal, A.K. Srivastava, Z.I. Maslova, S.M. Lebedka, Resiliency-driven strategies for power distribution system development, Electr. Power Syst. Res. (2021).
[45] V.V. Volokhin, I.M. Diahovchenko, B.V. Derevyanko, Electric energy accounting and power quality in electric networks with photovoltaic power stations, in: 2017 IEEE International Young Scientists Forum on Applied Physics and Engineering 2017, YSF, 2017 vol. 2017-Janua.
[46] I. Diahovchenko, N. Sushchenko, A. Shulumei, O. Strokin, Influence of supply voltage and frequency variations on the electrical equipment and power consumption in LV and MV distribution networks, Energetika (2019).
[47] J.M. Hernandez, P. Van Mieghem, Classification of graph metrics, Delft Univ. Technol. Mekelweg, Netherlands (2011).
[48] H. Kim, R. Anderson, Temporal node centrality in complex networks, Phys. Rev. E - Stat. Nonlinear, Soft Matter Phys. (2012).
[49] A. Yazdani, R.A. Otoo, P. Jeffrey, Resilience enhancing expansion strategies for water distribution systems: a network theory approach, Environ. Model. Softw. (2011).
[50] F. Meng, G. Fu, R. Farmani, C. Sweetapple, D. Butler, Topological attributes of network resilience: a study in water distribution systems, Water Res. (2018).
[51] A. Ganesh, L. Massoulié, and D. Towsley, "The effect of network topology on the spread of epidemics," in *Proceedings - IEEE INFOCOM*, 2005.
[52] P. Van Mieghem, J. Omic, R. Kooij, Virus spread in networks, IEEE/ACM Trans. Netw. (2009).
[53] F. Osmani, A. Kochov, Definition of indicators for decision-making to contribute to sustainable development through cleaner production and resource efficiency by using the AHP method, Energetika 64 (3) (2018) 155–166.
[54] L. Socaciu, O. Giurgiu, D. Banyai, M. Simion, PCM selection using AHP method to maintain thermal comfort of the vehicle occupants, Energy Procedia (2016).
[55] T.L. Saaty, Decision making with the analytic hierarchy process, Int. J. Serv. Sci. (2008).
[56] S.S. Silva, T.M.L. Assis, Adaptive underfrequency load shedding in systems with renewable energy sources and storage capability, Electr. Power Syst. Res. (2020).
[57] S. Fedorchuk, A. Ivakhnov, O. Bulhakov, and D. Danylchenko, "Optimization of storage systems according to the criterion of minimizing the cost of electricity for balancing renewable energy sources," in *2020 IEEE KhPI Week on Advanced Technology, KhPI Week 2020 - Conference Proceedings*, 2020.